IOP PUBLISHING PLASMA SOURCES SCIENCE AND TECHNOLOGY

Plasma Sources Sci. Technol. **22** (2013) 055021 (10pp) doi:10.1088/0963-0252/22/5/055021

Resonant RF network antennas for large-area and large-volume inductively coupled plasma sources

Ch Hollenstein[1], Ph Guittienne[2] and A A Howling[1]

[1] Ecole Polytechnique Fédérale de Lausanne (EPFL), Centre de Recherches en Physique des Plasmas, CH-1015 Lausanne, Switzerland

[2] HELYSSEN Sàrl, Route de la Louche 31, CH-1092 Belmont-sur-Lausanne, Switzerland

Received 25 February 2013, in final form 4 June 2013
Published 27 September 2013
Online at stacks.iop.org/PSST/22/055021

Abstract

Large-area and large-volume radio frequency (RF) plasmas are produced by different arrangements of an elementary electrical mesh consisting of two conductors interconnected by a capacitor at each end. The obtained cylindrical and planar RF networks are resonant and generate very high RF currents. The input impedance of such RF networks shows the behaviour of an *RLC* parallel resonance equivalent circuit. The real impedance at the resonance frequency is of great advantage for power matching compared with conventional inductive devices. Changes in the *RLC* equivalent circuit during the observed E–H transition will allow future interpretation of the plasma–antenna coupling. Furthermore, high power transfer efficiencies are found during inductively coupled plasma (ICP) operation. For the planar RF antenna network it is shown that the E–H transition occurs simultaneously over the entire antenna. The underlying physics of these discharges induced by the resonant RF network antenna is found to be identical to that of the conventional ICP devices described in the literature. The resonant RF network antenna is a new versatile plasma source, which can be adapted to applications in industry and research.

(Some figures may appear in colour only in the online journal)

1. Introduction

Resonant radio frequency (RF) network antennas are interesting new plasma sources with numerous potential applications in plasma processing as has recently been demonstrated [1, 2]. They show many advantages compared with the conventional capacitively coupled plasma or inductively coupled plasma (ICP) devices and could therefore replace these plasma reactors for certain industrial applications.

Resonant network antennas can be up-scaled without great difficulty to run as large-area or large-volume plasma sources with significantly less effort than the commonly used capacitive and inductive plasma sources. They can be adapted to the size and geometry of the optimal plasma volume for processing. RF power matching of the reactor is considerably easier due to the real impedance of the resonant network antenna. Consequently, the high RF currents or high RF voltages as observed in capacitive or inductive plasma reactors can be avoided. Furthermore, the impedance is only very weakly dependent on the antenna size and therefore does not lead to new complications when up-scaling.

In this paper, we demonstrate that resonant RF networks can be arranged to form large-area or large-volume plasma sources with properties similar to conventional ICP devices. As theoretical considerations [3] from the medical applications of birdcage coils and recent antenna design studies show, closed and open configurations of the antenna for plasma production are possible and can be described using the same mathematical formulation.

In this paper, we give examples of an open network antenna as a large-area planar plasma source and of a closed network antenna as a cylindrical plasma source. Both are composed of similar electrical meshes.

Low RF power operation of the planar RF network antenna driven at different normal modes is investigated in view of applications for surface treatment of large flat areas, such as film coating [4]. The cylindrical RF network antenna or

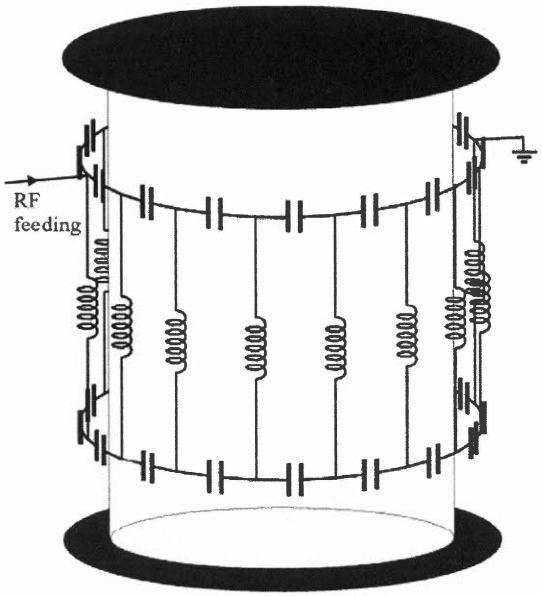

Figure 1. Schematic of the 16-leg cylindrical (birdcage) RF antenna, showing the electrical circuit and opposite points of RF feeding and grounding. The vacuum vessel is a glass cylinder closed at the top and bottom by grounded metal plates.

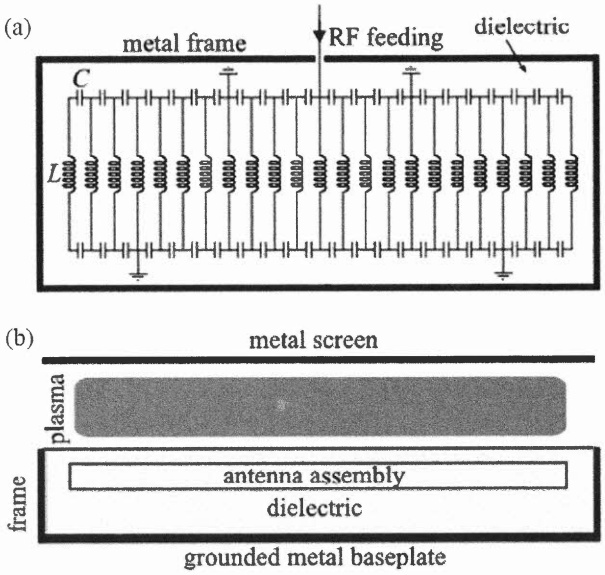

Figure 2. Schematic and electrical circuit of the 23-leg planar RF network antenna. (*a*) Top view showing the RF feeding point and the four ground connections. (*b*) Side view showing the metal screen used to confine the plasma above the antenna.

birdcage antenna has not yet been investigated for application as an ICP source. Operation at different normal modes shows the capability of this antenna type for large-volume plasma applications. The cylindrical plasma source can be used as a volume plasma source for immersion of many work pieces or for treatment of a large substrate. Other possible applications are plasma sources for neutral beam injectors in fusion devices, or for high-density ion thrusters. In both antenna cases, impedance measurements are useful in investigating the antenna–plasma interaction such as the E–H transition. The similarity of certain results for the two different plasma sources shows that it is possible to construct complex RF antennas out of the same basic network element, which can be adapted depending on the application.

Furthermore, the same resonant RF network antenna, which generates plasma by inductive coupling in the present case, can be further developed for wave-excited plasma sources since this type of antenna has been shown to efficiently excite helicon waves in the presence of a magnetic field [5]. Resonant RF network antennas are a new versatile type of antenna for large-area and large-volume plasma production as demanded by the growing plasma processing community.

2. Background of resonant network RF antennas

The closed birdcage coil shown in figure 1 is well known from nuclear magnetic resonance (NMR) applications where the uniform transverse RF magnetic field produced by the $m = 1$ mode is used to excite the nuclear spins within a sample. The structure and electrical properties of such a closed cylindrical birdcage antenna have been extensively described for the non-dissipative case in [3]. A planar antenna is made by unwrapping a birdcage coil to form a flat, open structure. The planar antenna can also be described as a segment of a ladder network, as shown in figure 2.

The theoretical background of the cylindrical and planar RF network antennas has already been described in the literature [3]. The calculation of the electrical circuit for the closed and open antennas is distinguished only by the boundary conditions inherent to their structure. By solving Kirchhoff's equations over the antenna with these corresponding boundary conditions, it is shown that resonant modes arise for both closed and open antennas. Each mode m is characterized by a resonance frequency determined by the distributed inductance and capacitance components and the mutual inductances, and by specific current and voltage distributions in the N antenna legs. The phase change per section is $2m\pi/N$ for the closed antenna, and $m\pi/N$ for the open antenna. The current and voltage amplitudes are sinusoidally distributed in space and are temporally in phase. The theoretical and measured current distributions in the legs of the cylindrical and planar antennas have been given in [1, 2].

In the neighbourhood of a mode resonance the impedance of the complex network antenna can be described by a parallel resonance r, L, C equivalent circuit. This general result applies to the cylindrical (closed) and planar (open) antennas, as demonstrated by the experiments described in this paper. The simultaneous measurement of RF current and voltage and their phase relation gives the antenna impedance and with this the equivalent circuit components r, L and C can be determined. The interpretation of the measured changes of these components caused by the plasma can therefore give insights into the plasma–antenna coupling, as will be discussed in future work.

An important aspect of proper RF antenna operation is the location of the RF feeding and grounding connections on the

antenna. There are a large number of different RF antenna arrangements possible in view of geometry and also in view of the RF operation and of the plasma obtained. In this paper, only one set of electrical connections is investigated for both antenna types. The influence of other connection schemes on the antenna behaviour and plasma operation is not discussed in this paper.

3. Experimental setup

Two different resonant RF network assemblies are investigated in this paper: a cylindrical and a planar RF antenna.

The cylindrical RF antenna was built following the concept of a high-pass birdcage coil [3]. The antenna was mounted outside a Pyrex glass tube of diameter 32 cm and length 50 cm. In figure 1, the RF antenna consists of 16 copper legs equally spaced by 6.7 cm interconnected with capacitors of 2.47 nF. The uncooled antenna was fed at the mid-point and operated usually with the opposite point grounded, as shown in the figure. These electrical connections favour the $m = 1$ mode structure of the birdcage antenna. Two half-cylinder screens could be mounted at a variable distance outside the antenna assembly to provide fine-tuning of the resonance frequency if a fixed excitation RF frequency was to be used [4]. The operating pressure range of the cylindrical RF network antenna was 10^{-3}–10^{-1} mbar in argon; the maximum RF power for this antenna assembly was 300–500 W.

The planar RF network antenna is built from elementary meshes composed of 20 cm-long copper rods and 2.6 nF capacitors similar to those used in previous works [1, 2]. The whole planar antenna, comprising 23 copper rods with 2.5 cm spacing as shown in figure 2, is placed inside a vacuum vessel of diameter 0.5 m and length 0.75 m. In order to avoid parasitic discharges, the antenna is embedded in a metallic box filled with silicone and covered on the plasma-facing side by a thin glass plate. Since the antenna is placed within the vacuum, the antenna–plasma distance (silicone plus glass plate) is only 5 mm, shorter than that in conventional ICP devices because a dielectric window thick enough to withstand atmospheric pressure is not necessary. A grounded screen was placed 7 cm in front of the antenna to define a discharge gap as typically encountered in plasma processing. The RF power was fed into the middle of the antenna whereas four points were grounded, as shown in figure 2, thus favouring the $m = 6$ mode. This planar RF network antenna corresponds to the electrical configuration used in previous investigations [1, 2]. The RF input power was limited to 200 W due to the RF current rating of the capacitors. However, by using a water-cooled antenna and parallel assemblies of capacitors to allow higher total currents, RF power up to 3 kW has already been used for coating applications [4]. The vacuum base pressure was 10^{-7} mbar and these experiments were also performed in argon at pressures of 10^{-3}–10^{-1} mbar.

A wideband power amplifier was used for tuning several antenna normal mode frequencies to investigate plasma operation at different normal modes. The frequency-dependent behaviour of the RF network antennas and of the resulting plasmas could thus be studied. The amplifier frequency range was 10–100 MHz, with a maximum power of 100 W, and a pi-matching circuit to connect the RF generator and the antenna.

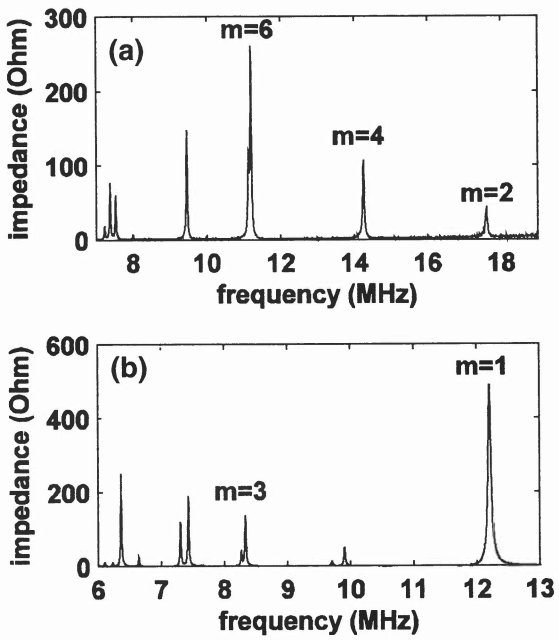

Figure 3. Magnitude of the impedance of the RF network antennas without a plasma, measured using a network analyser: (*a*) planar RF network antenna and (*b*) cylindrical (birdcage) antenna.

For electrical characterization of the RF network antennas without a plasma, a commercial RF network analyser was used, as shown in figures 3(*a*) and (*b*). During plasma operation, electrical characterization was performed using simultaneous measurements of RF voltage, RF current and their phase relation. Commercial voltage and current probes were used. The probes were mounted as close as possible to the RF antenna to minimize perturbations to the measured impedance. In this way, the antenna impedance for different normal modes was measured in the presence of a plasma. The frequencies around the normal mode resonances were scanned using the RF power amplifier. At each frequency step, the antenna was carefully matched to the RF generator. The high-frequency probes were calibrated by comparing impedance measurements with the RF network analyser measurements in the absence of a plasma. Figure 4 shows a typical electrical probe and network measurement of the impedance for the $m = 3$ normal mode of the cylindrical RF network. Note that the impedance and power input of the resonant antennas can easily be measured with sufficient accuracy using voltage and current probes, in contrast to highly reactive capacitive or inductive reactors for the following reason: for a conventional inductive or capacitive plasma source, it is difficult to measure the input impedance and power directly into the reactor using voltage, current and phase measurements at the reactor input, because the phase ϕ is very close to $+90°$ or $-90°$ for these reactive-impedance reactors. This means that the phase must be measured very accurately to avoid large errors in the measurement of power $= VI\cos(\phi)$ because $\cos(\phi)$ is close to zero and is very sensitive to small errors in the phase measurement. The matching

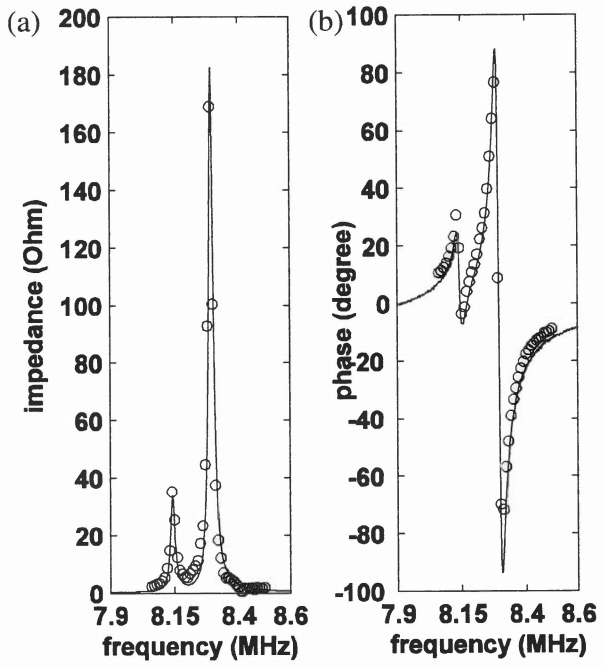

Figure 4. Comparison of network analyser impedance measurements (lines) with results obtained from RF voltage and RF current probe measurements (points) without a plasma (50 W) for the $m = 3$ mode of the cylindrical RF antenna: (*a*) magnitude and (*b*) phase.

box for these reactors transforms their reactive impedance to a resistive impedance (usually, close to 50 Ω) and so the power input to the matching box and the reactor system can be easily measured, but now the power measurement includes an unknown power loss in the matching box. The advantage of a resonant network plasma source is that the impedance and power measurements can easily be made directly at the reactor input (i.e. after the matching box), because the phase is close to zero and, therefore, the measurements are not very sensitive to small errors in the phase measurement.

As shown in previous works, the positions of the RF feed point and the grounded points of the cylindrical and planar antennas play a crucial role for the antenna and plasma operation [1, 2]. Several possible connection configurations can be chosen but a detailed study of their influence on the antenna operation and the produced plasma is beyond the scope of this paper. For this work, the above-mentioned connections of the RF feeding and grounding points of the cylindrical (figure 1) and planar (figure 2) antennas were kept the same for all results shown. For the cylindrical antenna, the connections for $m = 1$ operation were chosen, whereas for the planar antenna the same electrical connections ($m = 6$) as in the previous work [1, 2] were adopted. As a consequence, some of the modes exhibited very low input impedance.

For plasma diagnostics, Langmuir probes, light intensity and optical emission spectroscopy were used. Single and double Langmuir probes were applied to measure longitudinal and vertical density profiles and to detect the transition from a capacitively coupled discharge to an inductively driven discharge (E–H transition). The profile measurements were used to determine the uniformity of the plasma density and to test the proper operation of the antenna by comparison with the calculated electric and magnetic fields.

4. RF antenna characterization

Figure 3 shows the impedance of the planar and cylindrical antennas without a plasma as measured by a commercial RF network analyser. Both antennas show the presence of normal modes whose frequencies are determined by the antenna electrical components [1–3]. The reason for the fact that higher modes are found at low frequencies is that the chosen network is a high-pass circuit [3]. A simple parallel resonance *RLC* equivalent circuit can describe the impedance close to each normal mode frequency to a good approximation. The impedances, real at the resonance frequency, cover a range of up to several hundred ohms, a range favourable for efficient RF power matching, provided that the connection configuration is correctly chosen for the required mode. For a given resonance frequency, the RF current and RF voltage variations along the antennas were determined by RF probe measurements without a plasma. These distributions were used to determine the exact mode structure on the antenna. The mode numbers identified and investigated in the frame of this paper are indicated in figures 3(*a*) and (*b*) for the planar and cylindrical RF antennas, respectively.

The magnitude of impedance for the planar antenna operating at normal modes $m = 2$ and $m = 4$ in the presence of a plasma is shown for different pressures in figures 5 and 6. The antenna impedances were measured for different RF powers at each pressure. The magnitudes for the $m = 6$ mode look similar to those given in figures 5 and 6. The magnitude and phase of the impedances show the typical dependence of the impedance around the resonance frequency of an elementary *RLC* parallel resonance circuit. The magnitude of impedance at the resonance frequency is one of the main advantages of the present RF scheme compared with the usual inductive devices using solenoids or spiral coils. The normal mode frequency is slightly shifted towards higher frequency with increasing RF power and the real impedance decreases, indicating RF power dissipation in the plasma. The antenna resistance is reduced by a factor up to about 5. Figure 7 shows the impedance measurements for the cylindrical antenna, which basically shows the same behaviour of impedance as a function of the excitation frequency as the planar antenna. However, in this case the observed frequency shift in the presence of the plasma is larger than for the planar antenna. In addition, the frequency shift for the $m = 1$ mode is more pronounced than for the $m = 3$ mode.

Frequency shifts could be a disadvantage when using a fixed RF frequency generator in plasma processing, since the antenna impedance could shift out of the resonance condition as the power increases, leading to impedance mismatch and high reflected power if the shift is large. The frequency shift can be compensated using metallic screens mounted around the cylindrical antenna: by adjusting the screen–antenna distance, typically by about a centimetre, the normal mode frequency can be tuned to a fixed RF frequency power generator [4].

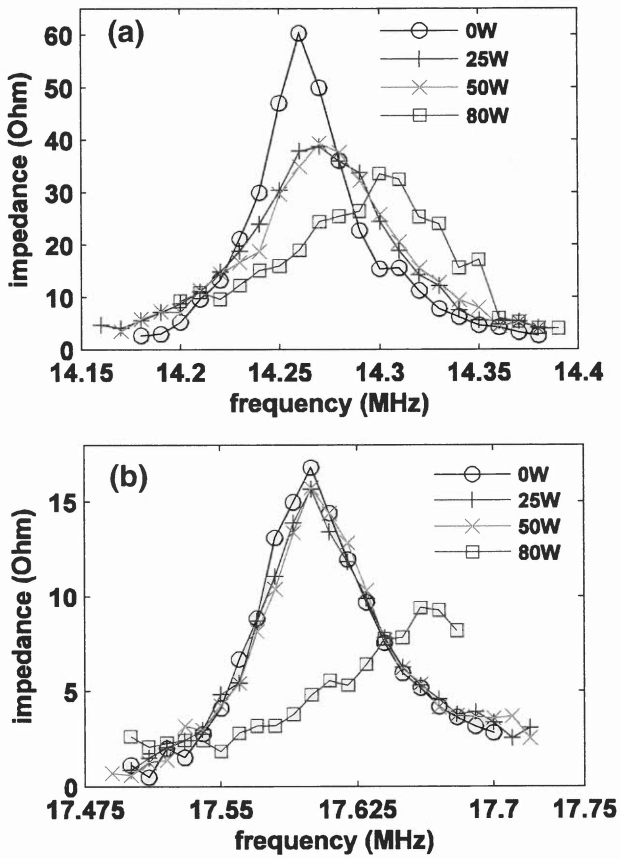

Figure 5. Impedance measurements: the magnitude of impedance for a planar RF network antenna at gas pressure 2×10^{-3} mbar as a function of the applied RF power: (*a*) $m = 4$ and (*b*) $m = 2$.

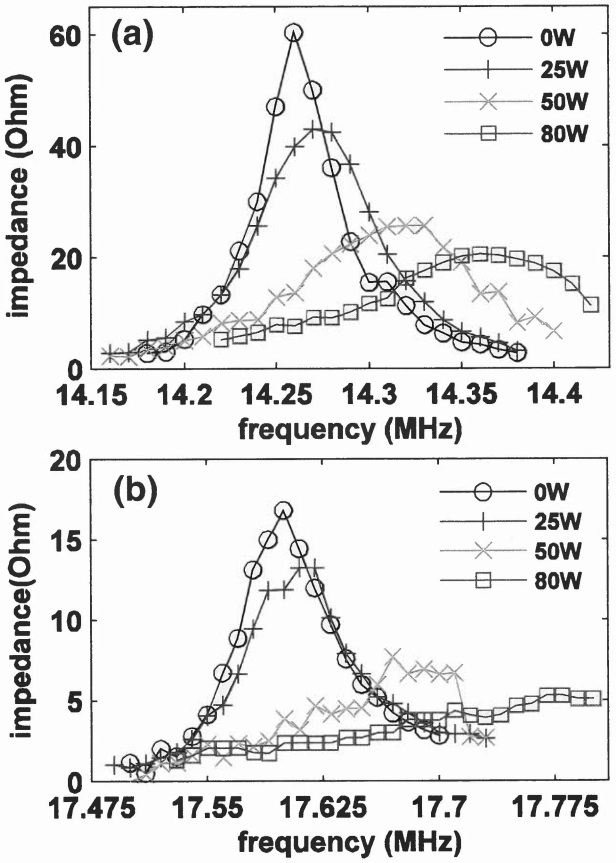

Figure 6. Impedance measurements: the magnitude of impedance for a planar RF network antenna at gas pressure 10^{-1} mbar as a function of the applied RF power: (*a*) $m = 4$ and (*b*) $m = 2$.

The influence of a metallic screen has also been observed in NMR applications and is based on mirror currents induced by the antenna in the metallic screen [3]. The frequency shifts for the planar antenna are much smaller and can be compensated in advance during the antenna construction by adjustment of the distance between the antenna and its metallic baseplate. Careful design of the planar antenna and its casing is an important factor for successful RF operation.

The real impedance of the antenna at a normal mode resonance frequency can be used to determine the power transfer efficiency to the plasma as follows: the impedance measurements presented above have shown that the input impedance of the antenna network in figure 1 or 2 behaves similarly to a parallel resonance circuit in the neighbourhood of a mode resonance. This means that the impedance near each resonance can be represented by an equivalent circuit of capacitance C in parallel with inductance L and resistance r. The values of C, L and r can be found by curve fitting to the experimental impedance measurements, and they have different fitted values for each resonance. The impedance of an r, L, C parallel resonance circuit is purely resistive at resonance and is given by

$$R_{\mathrm{vac}} = (\omega_{\mathrm{vac}}^2 C_{\mathrm{vac}} r_{\mathrm{vac}})^{-1}, \tag{1}$$

where R_{vac} is the input impedance measured in vacuum without a plasma, and $\omega_{\mathrm{vac}} = \sqrt{L_{\mathrm{vac}} C_{\mathrm{vac}}}$ is the angular frequency at the corresponding mode resonance. On plasma ignition, the power dissipation in the plasma due to coupling with the antenna manifests itself as an increase in r_{vac}, which is the dissipative element in the equivalent parallel resonance circuit. This is responsible for the fall in the antenna resonance input resistance, as shown by the inverse dependence between R and r in (1). More specifically, the ohmic resistance to current in the plasma is transformed by the antenna–plasma inductive coupling into an effective resistance in the antenna elements as described in [6], whose combined impedance results in the equivalent circuit resistance. Explicit expressions for the relations between the plasma resistance, the antenna element resistances and the combined equivalent circuit resistance would require further analysis, but the equivalent circuit description is sufficient for our purposes in this paper.

The resonance frequency is observed to increase by $\delta\omega$ in the presence of a plasma. Since the equivalent circuit capacitance C_{vac} is dominated by the antenna capacitors whose capacitance is substantially larger than any antenna–plasma sheath capacitive coupling, we will assume here that the mode frequency increase, $\delta\omega$, is due to a decrease in L_{vac}. In the presence of a plasma, equation (1) therefore becomes

$$R_{\mathrm{load}} = (\omega_{\mathrm{load}}^2 C_{\mathrm{load}} r_{\mathrm{load}})^{-1}, \tag{2}$$

where R_{load} is the reduced input impedance when the antenna is loaded by coupling to the plasma, $\omega_{\mathrm{load}} = \omega_{\mathrm{vac}} + \delta\omega$, r_{load}

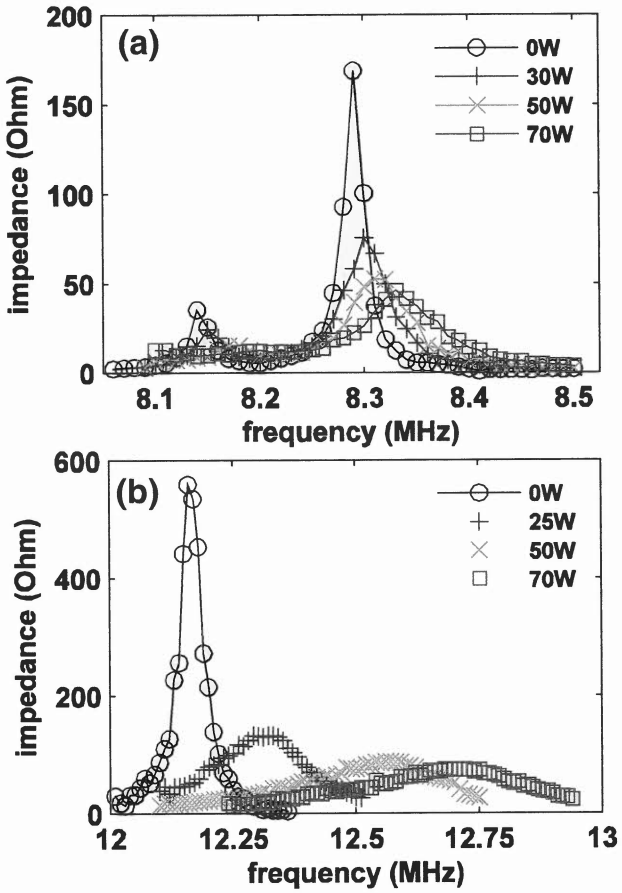

Figure 7. Impedance measurements: the magnitude of impedance for a cylindrical RF network antenna at gas pressure 10^{-1} mbar as a function of the applied RF power: (*a*) $m = 3$ and (*b*) $m = 1$.

is the increased equivalent resistance due to plasma coupling, and the capacitance is unchanged, $C_{\text{load}} = C_{\text{vac}}$. Finally, the power transfer efficiency η from the antenna to the plasma is given by the fraction of the equivalent resistance due to the plasma coupling, i.e.

$$\eta = \frac{r_{\text{load}} - r_{\text{vac}}}{r_{\text{load}}} = 1 - \frac{\omega_{\text{load}}^2 R_{\text{load}}}{\omega_{\text{vac}}^2 R_{\text{vac}}} \approx 1 - \frac{R_{\text{load}}}{R_{\text{vac}}}\left(1 + 2\frac{\delta\omega}{\omega_{\text{vac}}}\right), \quad (3)$$

using (1) and (2), where $\delta\omega$ is the frequency shift due to the plasma, and R_{vac} and R_{load} are the measured antenna real impedances at resonance in vacuum, and with the plasma, respectively. Figure 8 shows the obtained power transfer efficiencies of the planar and cylindrical RF antennas operated at different normal modes. Both RF network antennas show a power transfer efficiency of 70–90% for the inductively driven discharge obtained at higher RF powers. These values are comparable to power transfer efficiencies of conventional ICP devices [6]. Resonant RF network antennas are therefore as efficient as the conventional ICP sources investigated in the literature.

Furthermore, from the frequency dependence of the impedance changes due to the plasma, the equivalent

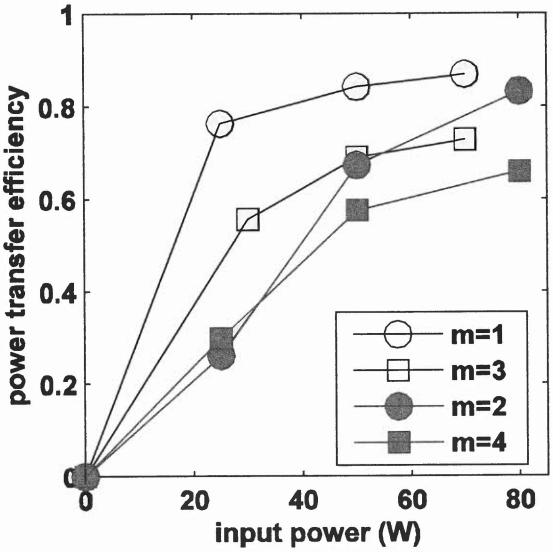

Figure 8. Measured power transfer efficiency for the cylindrical RF antenna ($m = 1$, $m = 3$; $p = 10^{-2}$ mbar) and for the planar RF network antenna ($m = 2$, $m = 4$; $p = 2 \times 10^{-3}$ mbar).

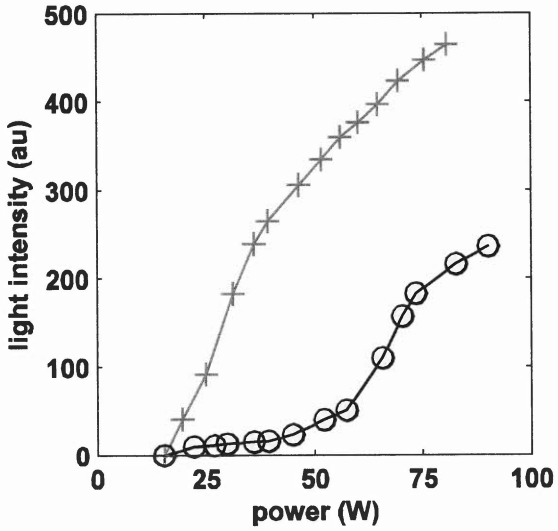

Figure 9. Visible light intensity versus RF power. Planar RF network antenna for mode $m = 2$ ((+) 10^{-2} mbar, (o) 2×10^{-3} mbar).

capacitance, inductance and resistance can be determined using the r, L, C equivalent circuit model. However, before the mechanisms of antenna–plasma interactions can be elucidated, these impedance changes must first be related to changes in the antenna component values in figures 1 and 2. Antenna modelling to understand the relation between the equivalent circuit impedances and the antenna component impedances is underway.

5. Plasma characterization

Single Langmuir probes and visible light emission were used to monitor the transition from a capacitively coupled discharge to an inductively coupled discharge as the RF power is increased, as also observed in conventional ICP devices [7, 8]. Figure 9

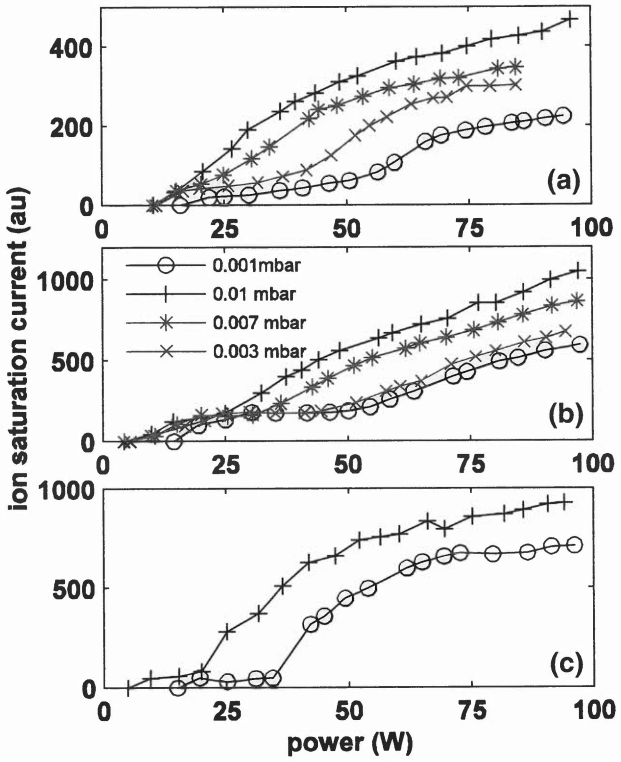

Figure 10. Ion saturation current versus RF power for various pressures in the case of the planar RF network antenna: (*a*) $m = 2$, (*b*) $m = 4$ and (*c*) $m = 6$.

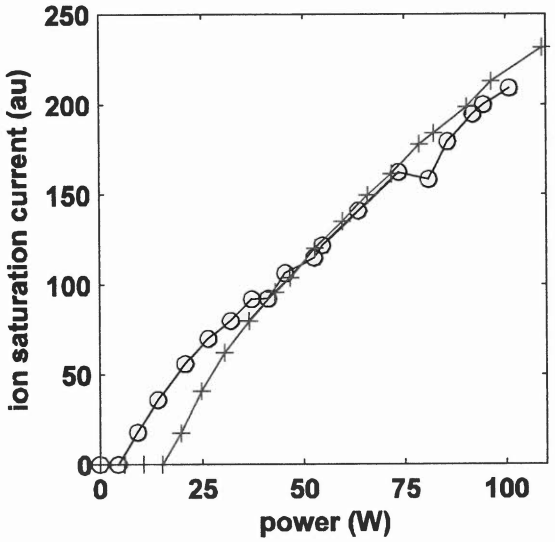

Figure 11. Ion saturation current versus RF power for the cylindrical RF network antenna at 10^{-1} mbar: (o) $m = 1$ and (+) $m = 3$.

shows the visible light intensity as a function of the RF power for two gas pressures for the $m = 2$ mode of the planar antenna. A jump in the light intensity is an indication that the discharge underwent a transition from a capacitively coupled discharge to an inductively coupled discharge. At low gas pressures, the E–H transition occurs typically around 60–70 W whereas at higher gas pressures, the RF power for transition is around 20 W. Similar results were obtained for all investigated modes and gas pressures, for the planar and also for the cylindrical RF antenna.

The measurements of the ion saturation current also show a typical change around the same RF power as for the visible light intensity. In figure 10 the ion saturation current is shown as a function of the RF power for different gas pressures and normal modes ($m = 2$, 4 and 6). In all cases, a typical jump in the ion saturation current is observed. For all three of the normal modes investigated for the planar RF antenna, the jump appears at a lower RF power for higher gas pressures. Similar behaviour of the ion saturation current can also be observed for the normal modes of the cylindrical RF antenna, as shown in figure 11. The clear jump in the ion density and also in the light emission (not shown) indicates a transition of the discharge. All these observations are in close agreement with reported observations of the so-called E–H transition in conventional ICP devices [7, 8].

The impedance at the resonances presented in figures 5 and 6 shows only a small reduction in the antenna equivalent circuit resistance for low RF powers, whereas at higher RF powers, substantial resistance reductions are found for all the normal modes investigated. Using equation (1), this leads to the conclusion that the RF power transfer efficiency is low during the initial, capacitively dominated phase, as shown in figure 8. Only a small amount of RF power is absorbed in the discharge during the capacitive phase. High power transfer efficiencies are obtained only after the transition to the inductively dominated plasma phase.

All these experimental observations clearly indicate that, at low RF powers, both types of RF network antennas create a capacitively coupled plasma, whereas at higher RF powers, a transition occurs towards a fully inductively coupled discharge. This behaviour is thus identical to that found in conventional ICP devices [6–11].

Other electrical quantities are also influenced by the transition from a capacitively to an inductively coupled discharge. As can be seen in figures 5–7, the frequency shift of the resonance is small for low RF power capacitively coupled discharges. At a higher RF power, larger frequency shifts are observed. The frequency shift can be due to changes in the equivalent circuit capacitance and/or inductance. However, the antenna capacitance is substantially bigger than the plasma sheath capacitance, so that the plasma does not directly influence the total antenna capacitance. Therefore, the observed increase in frequency is due to a reduction in the antenna equivalent circuit inductance, which can be attributed to inductive coupling. A dissipative network model is currently being developed to interpret these measurements in terms of the effect of plasma coupling on the antenna component values.

Spatial profiles of the ion saturation current were measured in both RF antenna systems. Density profiles are useful in examining the correct operation of the antenna in terms of power distribution corresponding to the driven mode, and in measuring the uniformity of the ion density, which is an important parameter for industrial applications. Longitudinal (axial) and transverse (radial) ion saturation profiles were measured for the planar (cylindrical) antennas, respectively. In figures 12(*a*) and (*c*), longitudinal profiles for the planar

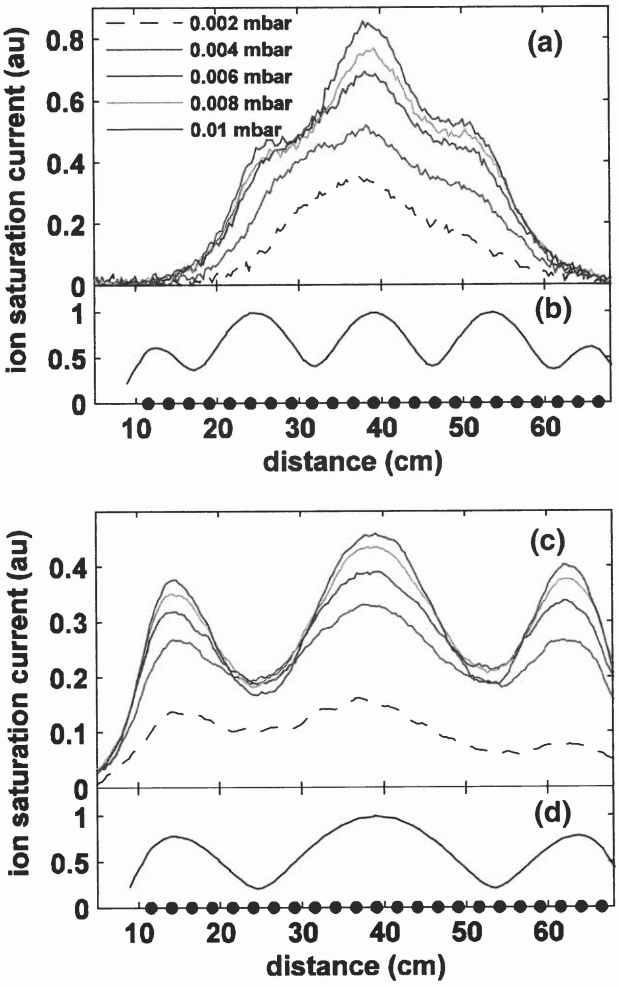

Figure 12. Longitudinal ion saturation current profiles, measured 2 cm above the planar antenna, for different pressures, modes (*a*) $m = 4$ and (*c*) $m = 2$ at 50 W RF power. The circles in (*b*) and (*d*) mark the positions of the antenna legs, and the trace gives the normalized magnitude of the calculated magnetic field 2 cm above the antenna.

antenna are shown for modes $m = 4$ and $m = 2$ for different gas pressures. Figures 12(*b*) and (*d*) show the calculated magnetic field produced by the corresponding mode structure. The three local density maxima in figure 12(*c*) correspond to the regions of maximum RF current flowing in the antenna, corresponding to the mode $m = 2$. This is also the case for the $m = 4$ mode operation in figure 12(*a*), but due to the particular distribution of the RF current maxima within the antenna, a narrower, more peaked density profile is observed. The similarity of the profiles shows that the plasma density develops simultaneously over the whole antenna, as is also the case when the RF power increases in figure 13(*a*): At a low RF power, a capacitively coupled discharge is produced everywhere, and also, at a higher RF power, the transition to an inductive discharge occurs over the entire antenna, as shown by figure 13(*b*). A complete study of the density profiles obtained for the planar RF antenna shows that the choice of the mode number, and also of the antenna internal electrical connections, all strongly influence the uniformity of the ion density, at least

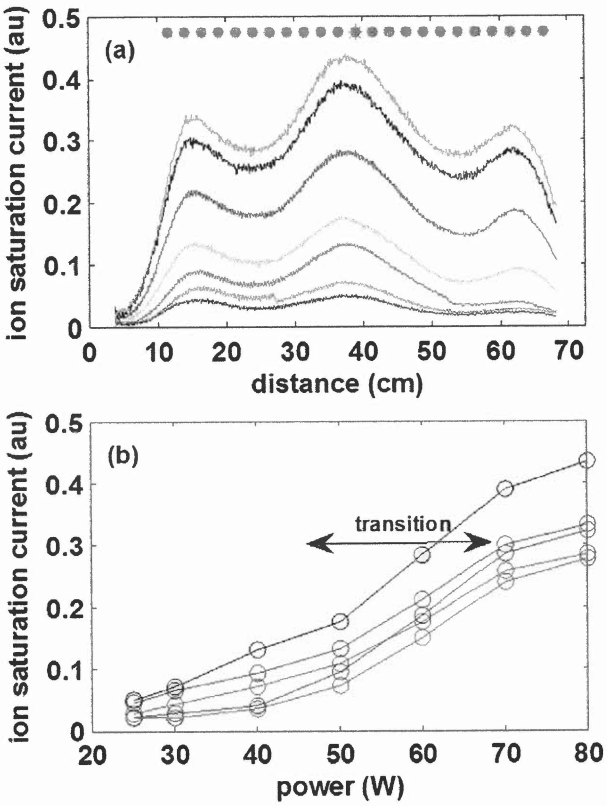

Figure 13. (*a*) Longitudinal ion saturation current profile for the planar RF network antenna in mode $m = 2$ as a function of the RF power (25, 30, 40, 50, 60, 70, 80 W), and (*b*) ion saturation current versus RF power taken at positions 15, 24, 39, 54 and 63 cm in (*a*).

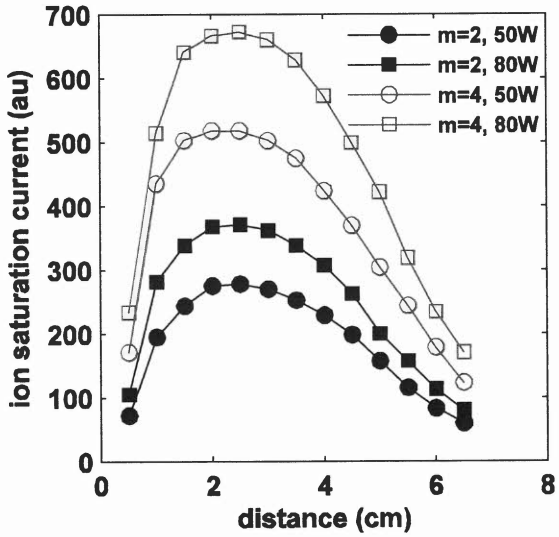

Figure 14. Transverse profile of the ion saturation current versus distance above the planar antenna for modes $m = 2$ and $m = 4$.

for these low RF powers. At higher RF powers, more uniform density profiles are always observed [1].

Transverse profiles of the ion saturation current measured in the 7 cm gap above the planar antenna are presented in figure 14 for $m = 2$ and $m = 4$ at different RF powers. At low

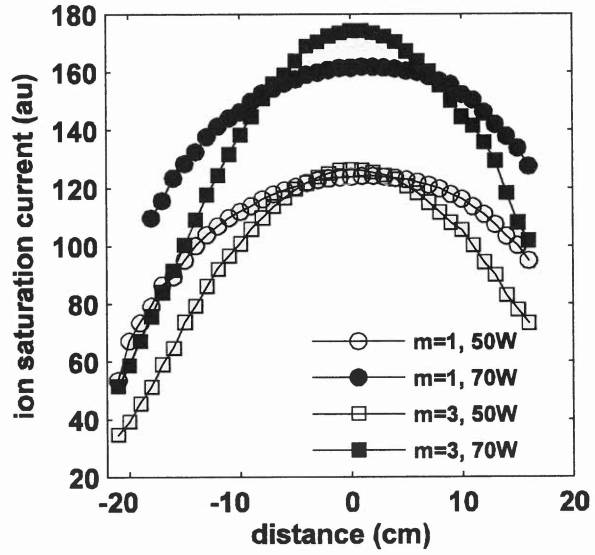

Figure 15. Axial ion saturation current profiles for the cylindrical antenna ($p = 10^{-1}$ mbar).

pressures and RF powers, rather symmetric ion saturation profiles are observed, a sign of the capacitive nature of the discharge. At higher pressures and RF powers, the maximum of the profile is slightly shifted towards the antenna, indicating an inductively driven discharge. The position of the ion density maximum roughly coincides with the calculated skin depth. Profile measurements show similar behaviour for different gap sizes. If there is no metal screen to confine the plasma above the planar antenna, the plasma fills the whole vacuum chamber. An arrangement of several planar plasma sources inside the cylindrical vacuum vessel wall could therefore also be used to obtain a very large volume plasma.

Axial ion density profiles for the cylindrical RF antenna are shown in figure 15 for $m = 1$ and $m = 3$ for different RF powers. The behaviour of the other modes and more detailed investigations into the influence of the mode structure on the plasma are currently underway. Within the RF power range limited by the present design of the RF antennas, double Langmuir probe measurements of the plasma showed that electron densities of a few $10^{16}\,\mathrm{m}^{-3}$ at 140 W with a typical electron temperature of approximately 2.5 eV could be produced by the cylindrical RF antenna.

The azimuthal ion saturation profile for the cylindrical RF antenna operated at $m = 1$ is shown in figure 16(*a*). The profile shows the same behaviour as the calculated normalized magnitude of magnetic field produced by the coil (figure 16(*b*)). The magnitude of the magnetic field was calculated for the case of vacuum with the COMSOL software. The fine structure of the magnetic field is due to the different legs of the birdcage coil. Finally, figure 17 shows the radial ion saturation profile of the plasma produced by the cylindrical antenna. The antenna was used in the $m = 1$ mode at an RF power of 65 W at 4×10^{-2} mbar. The radial profile reveals a rather constant ion saturation current in the middle of the discharge, whereas most inductively coupled discharges have more or less pronounced hollow density profiles.

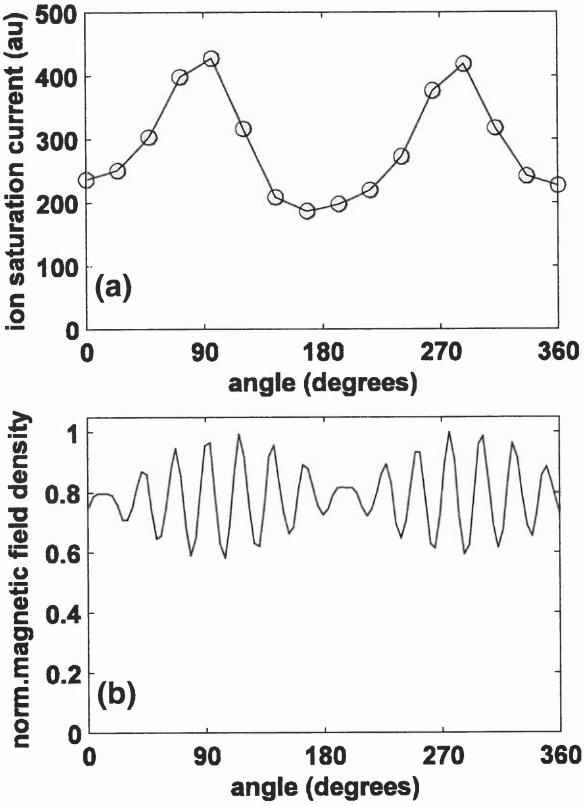

Figure 16. (*a*) Azimuthal profile of the ion saturation current in the plasma of the cylindrical antenna at $R = 16$ cm ($m = 1$, $P_{\mathrm{rf}} = 65$ W, $p = 4 \times 10^{-2}$ mbar). (*b*) Calculated normalized magnetic flux density at the same radial position as the ion saturation profile in (*a*).

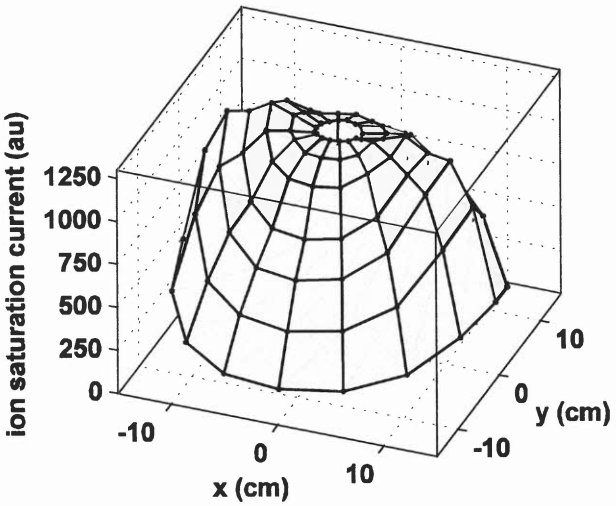

Figure 17. Radial ion saturation current profile at the mid-plane of the cylindrical antenna ($m = 1$, $P_{\mathrm{rf}} = 65$ W, $p = 4 \times 10^{-2}$ mbar).

6. Conclusion

Large-area and large-volume RF plasma sources can be built up using different arrangements of the same elementary electrical meshes to form planar, cylindrical or even other shapes of resonant RF network antennas. A typical example of an elementary mesh consists of two conductors interconnected

by a capacitor at each end. When driven at one of its resonant frequencies, very high currents are generated within the antenna structure. A resonant RF network antenna can therefore be used as a source for an inductively coupled plasma, which can be scaled up to large areas or large volumes more easily than for conventional sources [12]. The input impedance of all the various antennas, close to a normal mode resonance, shows the characteristics of an *RLC* parallel resonance equivalent circuit. At a resonance frequency, the antenna presents a real input impedance, thus facilitating matching to RF power generators. Changes in the *RLC* equivalent circuit values due to coupling with the plasma can be used to determine plasma parameters, for example, a simple estimation of the power transfer efficiency.

The plasmas produced by these antennas show the transition from the capacitively coupled to the inductively coupled regime as found in conventional ICP devices using solenoids or spiral coils. The underlying physics of discharges driven by the resonant RF network antenna is essentially the same. The E–H transition occurs simultaneously over the entire antenna. Therefore, it is expected that for both antenna types similar performances and plasma parameters as for conventional ICP sources can be reached.

The resonant RF network can be used to construct a wide variety of RF antennas. A large-area planar antenna has already been successfully used in the packaging industry [4] and other interesting applications to other plasma processes are in preparation. With addition of an external magnetic field, the network antenna also opens the way to new wave-excited plasma sources. The resonant RF network antenna is an important new plasma source, which can be adapted to applications in research and industry.

Acknowledgments

The Swiss Commission for Technology and Innovation (Grant No 9896.2 PFIW-IW) supported part of this work. In addition, the authors would like to thank the CRPP and CRPP staff for their excellent support.

References

[1] Guittienne Ph, Lecoultre S, Fayet P, Larrieu J, Howling A A and Hollenstein Ch 2012 Resonant planar antenna as an inductive plasma source *J. Appl. Phys.* **111** 083305

[2] Lecoultre S, Guittienne Ph, Howling A A, Fayet P and Hollenstein Ch 2012 Plasma generation by inductive coupling with a planar resonant RF network antenna *J. Phys. D: Appl. Phys.* **45** 082001

[3] Jin J 1998 *Electromagnetic Analysis and Designs in Magnetic Resonance Imaging* (Boca Raton, FL: CRC Press)

[4] Guittienne Ph, Fayet P, Larrieu J, Howling A A and Hollenstein Ch 2012 Plasma generation with a resonant planar antenna *55th Annual SVC (Surface Vacuum Coaters) Technical Conf. (Santa Clara, CA, 28 April–3 May 2012)*

[5] Guittienne Ph, Chevalier E and Hollenstein Ch 2005 Towards an optimal antenna for helicon waves excitation *J. Appl. Phys.* **98** 083304

[6] Piejak R B, Godyak V A and Alexandrovich B M 1992 A simple analysis of an inductive RF discharge *Plasma Sources Sci. Technol.* **1** 179

[7] Cunge G, Crowley B, Vender D and Turner M M 1999 Characterization of the E-to-H transition in a pulsed inductively coupled plasma discharge with internal coil geometry: bi-stability and hysteresis *Plasma Sources Sci. Technol.* **8** 576

[8] Kortshagen U, Gibson N D and Lawler J E 1996 On the E–H mode transition in RF inductive discharges *J. Phys. D: Appl. Phys.* **29** 1224

[9] Godyak V 2003 Plasma phenomena in inductive discharges *Plasma Phys. Control. Fusion* **45** A399

[10] Lieberman M A and Boswell R W 1998 Modeling the transition from capacitive to inductive to wave-sustained rf discharges *J. Phys. IV* **8** Pr7-145

[11] Zhao S-X, Xu X, Li X-C and Wang Y-N 2009 Fluid simulation of the E–H transition in inductively coupled plasma *J. Appl. Phys.* **105** 083306

[12] Wendt A E and Mahoney L J 1996 Radio frequency inductive discharge source design for large area processing *Pure Appl. Chem.* **68** 1055